This article has been accepted for publication in a future issue of this journal, but has not been fully edited. Content may change prior to final publication. Citation information: DOI 10.1109/TNANO.2015.2471298, IEEE Transactions on Nanotechnology

Temperature Control for Nano-Scale Films by Spatially-Separated Atomic Layer Deposition based on Generalized Predictive Control

Wen-Jie He, *Student Member, IEEE,* Hai-Tao Zhang, *Senior Member, IEEE,* Zhiyong Chen, *Senior Member, IEEE,* Ji-Long Lin, Kan Tian, Bin Shan, and Rong Chen, *Member, IEEE*

***Abstract*—This paper established a closed-loop temperature control system for a spatially-separated atomic layer deposition (S-ALD) reactor using generalized predictive control (GPC) algorithm. The GPC-based closed-loop control system rapidly and precisely stabilized the reactor temperature in the presence of thermal field disturbances. Compared with the proportion integration differentiation (PID) control commonly used for S-ALD, the closed-loop GPC system attenuated reaction temperature oscillations when producing two-element nano-scale thin films. Furthermore, the proposed GPC system demonstrated the superiority in multi-element nano-laminates depositing efficiency by reducing the settling time with a substrate moving between different reactors. Electrical and optical properties of films verified the feasibility of the proposed GPC system. Finally, experimental results presented that the microstructure of the deposited ALD nanometer thin film was improved with the developed GPC system, compared with PID strategy.**

***Index Terms*—Atomic layer deposition, predictive control, temperature control.**

I. Introduction

ATOMIC layer deposition (ALD) is a thin film preparation technique relying on sequential self-limiting surface chemical reactions to produce nano-scale films [1–3]. The surface-reaction saturation nature enables precise control of film thickness, conformality, and uniformity over large areas, enabling applications in the fields of microelectronics, environmental protection, renewable energy, etc. [4–7]. ALD has shown great capabilities in depositing metallic and bi-elemental compound films, meanwhile nano-laminates recently have attracted more and more attentions, due to their unique electrical and optical properties [8]. ALD is well accepted in preparing such structures of different materials with respective layer thicknesses in the same reactor. However, to date, both for two-element compounds and nano-laminate structures, the conventional batch-mode ALD system is still far from large-scale and continuous production. The reason lies in inert gas purge processes removing the surplus precursors and by-products during each reaction cycle.

In this situation, spatially-separated ALD (S-ALD) is thus developed for large scale and continuous deposition [9, 10]. In an S-ALD system, different precursors fill in corresponding physical zones with inert gas inlets installed between precursor injectors to prevent the cross contamination and atmosphere perturbation. During deposition processes, a film is formed on a substrate when the substrate moves back and forth under precursor injectors, in which by-products are purged when the substrate passes through an inert gas diffusion barrier after each ALD half-reaction. Upon alternately adding several injectors for precursor and separation, a key feature of the S-ALD is its high deposition rate, which can reach more than 1.2 nm/s [11]. Moreover, it could deposit nano-laminate films or multi-element compound thin films produced by different precursor sources. Another merit of the S-ALD process is its feasibility at normal atmospheric pressure condition, which remarkably reduces the production cost in large-scale and high-efficiency manufacturing fields. For instance, the S-ALD system could deposit the Al_2O_3 films as surface passivation layers with 1.2 nm/s in solar cell [12, 13], as well as the ZnO films to act as transparent and conducting films [14, 15].

Similar to temporal ALD technology [16], temperature is also a key process factor that greatly influences both the quality of films and the processing efficiency in S-ALD processes. In an ALD run susceptible to thermal field disturbances, the temperature is required to rapidly recover to the target value to avoid reactants decomposition and vapor phase side reactions. Moreover, reaction temperature control is also crucial to guarantee the uniformity of the film thickness [1]. Different from temporal ALD, S-ALD is usually an open system with high gas flow rate, which easily results in the temperature oscillations. Specifically, in an S-ALD system, both the precursor mixed with carrier gas and inert gas will

This work was supported by the National Basic Research Program of China under Grant 2013CB934800, the Hubei Province Funds for Distinguished Young Scientists under Grant 2015CFA034 and 2014CFA018, the National Natural Science Foundation of China under Grants 51575217, 51572097, 61322304 and 51120155001, the Thousand Young Talents Plan, the Recruitment Program of Global Experts, the Fundamental Research Funds for the Central Universities of HUST under Grant 2014TS037, and the Program for Changjiang Scholars and Innovative Research Team in University under Grant IRT13017. (*Corresponding authors: R. Chen, and H.-T. Zhang.*)

W.-J. He, J.-L. Lin and R. Chen are with State Key Laboratory of Digital Manufacturing Equipment and Technology, School of Mechanical Science and Engineering, Huazhong University of Science and Technology, Wuhan 430074, China (email: rongchen@mail.hust.edu.cn)

H.-T. Zhang is with the Key Laboratory of Image Processing and Intelligent Control, School of Automation, and State Key Laboratory of Digital Manufacturing Equipment and Technology, Huazhong University of Science and Technology, Wuhan 430074, China (email: zht@mail.hust.edu.cn)

Z. Chen is with the School of Electrical Engineering and Computer Science, University of Newcastle, Callaghan, NSW 2308, Australia.

K. Tian is with the China-EU Institute for Clean and Renewable Energy, Huazhong University of Science and Technology, Wuhan 430074, China.

B. Shan is with the State Key Laboratory of Material Processing and Die and Mould Technology, School of Materials Science and Engineering, Huazhong University of Science and Technology, Wuhan 430074, China.

This article has been accepted for publication in a future issue of this journal, but has not been fully edited. Content may change prior to final publication. Citation information: DOI 10.1109/TNANO.2015.2471298, IEEE Transactions on Nanotechnology

perturb the reactor temperature. Meanwhile, the flow region of precursors and inert gas is unevenly distributed in the reaction zone due to the substrate moving back and forth. The inherent temperature oscillations and uneven distribution of the thermal field inevitably worsen the deposition reaction. Moreover, the growth of some nano-laminates requires substrate moving between different ALD temperature windows. The substrate temperature needs to reach the desirable set-point ranges between different reactors. Thus the film deposition efficiency largely depends on the switching and settling times of the substrate temperature control systems. Therefore, it becomes a challenging task to develop an effective temperature controller for S-ALD systems.

Model predictive control (MPC) is regarded as a mainstream control method in many industrial processes [17, 18], especially in chemical process control and energy system control applications [19–22]. Generalized predictive control (GPC) [23], as a representative of MPC, has shown its effectiveness in process control and reactor temperature control [24] due to the model prediction mechanism based on the controlled autoregressive integrated moving average (CARIMA) model [25]. Furthermore, both the receding horizon optimization and the output rectification improve GPC robustness to external disturbances and dynamics uncertainties. To date, there are few works on conventional batch-mode ALD reactor temperature control using a GPC method. For example, in a conventional ALD reactor, we have designed a GPC-based temperature control system reported in a recent paper [16].

However, GPC-based control strategy has not yet been used for an S-ALD reactor. There are several major challenges for the controller development of an S-ALD reactor compared with that for a conventional ALD reactor: i) S-ALD is exposed to the air and hence easily affected by environment disturbances; ii) A moving substrate makes it hard to distribute sensors and actuators in an extremely narrow gap (micron level) between the injectors and the substrate; iii) In a conventional ALD reactor, the controlled object is statically located on one heating source. But in an S-ALD reactor, it switches back and forth between two heaters particularly when depositing nano-laminate films; iv) Conventional ALD is in batch mode, so external disturbances are mainly in step form caused by loading/unloading samples. S-ALD is a kind of continuous processing, so external disturbances persistently exist. More specifically, due to the uneven gas flow distribution, the moving substrate and the exposure of the micro-gap to atmosphere, disturbances inevitably exist including flow rate pulses, the gas flow rate variations and the switches of substrate moving direction.

With the development of the S-ALD technology, it becomes more desirable to establish a closed-loop temperature control system with sufficiently small temperature oscillations, short settling time, and strong robustness with respect to thermal disturbances induced by moving substrate. In this work, we hereby develop a GPC-based closed-loop control system to fulfill such an urgent yet challenging task so as to facilitate film production in an S-ALD reactor.

This paper is organized as follows. Section II introduces the developed S-ALD platform and the detailed S-ALD procedures. In Section III, the effectiveness and robustness of the proposed GPC system are examined by experiments with various moving speeds. In Section IV, the temperature control performances of GPC and PID are compared to show the superiority of the former. In Section V, the effectiveness of the proposed GPC system is further verified by experiments of nano-laminate film deposition. Finally, conclusions are drawn in Section VI.

II. S-ALD System Description

As shown in Fig. 1(a), it is a minimal unit to activate a complete ALD reaction. A two-element compound thin film is deposited by the substrate moving back and forth within the unit. Since the motor halts and switches the direction at both ends of the unit, the depositing time increases. Fortunately, the depositing efficiency can be improved through expanding a single unit to multiple serial units. In this way, the ALD deposition cycle number is equal to the unit number, just within a single direction movement. Indeed, there are several switching points within the same deposition loop for only one ALD unit. Another virtue of the unit expansion is the continuous injection of different precursors. Thus a two-element compound thin film with a certain thickness can be deposited in one unit, and the substrate afterwards moves to the other unit area to complete the loops to form a film with laminate structure finally. To this end, we have developed an S-ALD platform with one unit as shown in Fig. 1(b). The platform includes a gas manifold, a reactor, a motor and an elevator. The gas manifold section consists of Swagelok 1/4" tubes, double-way precursor bottles, ball valves, and mass flow controllers (MFCs) for maintaining the flow rates of both the carrier gas and the inert gas for diffusion barrier. The reactor section contains several injectors which transmit precursors and separated inert gas into the reaction area and the sample holder of the substrate onto the heater. The temperature on the substrate surface is monitored by a platinum resistance needle sensor whose signal is transmitted to a PLC A/D module. The substrate of the S-ALD platform is driven by a stepper motor to move along with the heater between the injectors of the precursors. The motor is controlled by an Arduino board. The elevator is used to adjust the gap between the lower surfaces of the injectors and the substrate. The software used is LabVIEW 2010.

During an S-ALD process, precursor vapor is continuously carried out of the precursor's bottle by the inert gas, and then mixed with the abundant inert gas in the bubbler of the bottle. Afterwards, the mixture vapor is transmitted into the corresponding injector. Once the substrate temperature reaches a prescribed range at the first deposition, the ALD growth reaction is activated. Unlike the conventional temporal ALD [3], the purge process is completed when the substrate passes through the inert gas diffusion barrier zone between the precursor zones in the S-ALD platform. Significantly, the precursors are continuously injected, and the substrate keeps moving between the two ends. Meanwhile, the mixture of carrier gases with precursors, and the inert gases for barrier are continuously fed into injectors. Before depositing a compound

This article has been accepted for publication in a future issue of this journal, but has not been fully edited. Content may change prior to final publication. Citation information: DOI 10.1109/TNANO.2015.2471298, IEEE Transactions on Nanotechnology

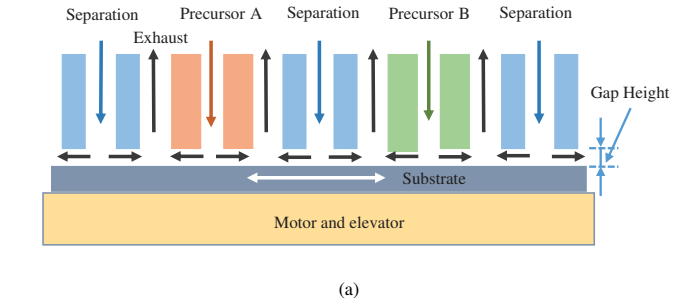

(a)

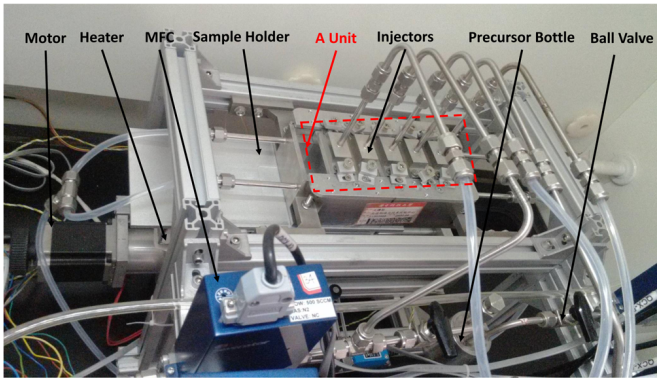

(b)

Fig. 1. The spatially-separated ALD: (a) reactor structure (b) real reactor.

film, the substrate is preheated to a desired temperature, and then moves into the reactor where the precursor and the inert purging gas keep a constant flow into the corresponding injector zones. Therefore, during the entire S-ALD process, the loading/uploading of samples would not destroy gas flow atmosphere or the deposition status. The substrate moving speed determines the time of the thin film deposition with desired thickness, while too high speed may destroy the steady state of gas distribution in the reaction zone. Since the substrate temperature sensor moves along with the substrate, the measured temperature is inevitably affected by the moving speed. So it is essential to establish a GPC-based closed-loop temperature control system to minimize the disturbances induced by the moving substrate. Here we have established such a closed-loop system, where the temperature and mass flow rate are both measured and transmitted to Siemens PLC series. Then the PLC program communicates with a PC through a serial port, and calculates the feedback control law by an OLE for Process Control (OPC) module.

III. Temperature Control Experiments to Produce Two-Element Compound Films

In this section, we carry out a two-element compound thin film deposition experiment in one ALD unit or several sequential identical units.

A. Modeling and prediction

The S-ALD reactor can be represented by the following state-space model

$$\begin{aligned} x(t+1) &= Ax(t)+Bu(t), \\ y(t) &= Cx(t), \end{aligned} \tag{1}$$

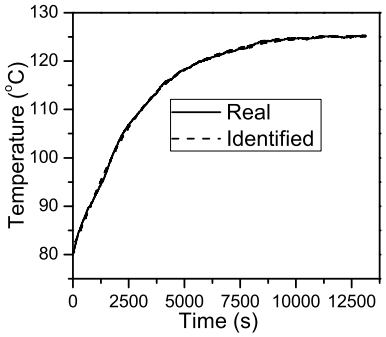

Fig. 2. Step response curve of system identification.

where $x(t) \in \mathbb{R}^n$ is the state vector, $u(t), y(t) \in \mathbb{R}$ are the input heater voltage and output substrate temperature, respectively, $A \in \mathbb{R}^{n\times n}$ and $B, C^\intercal \in \mathbb{R}^n$.

By implementing a 3.5 V-DC step-response experiment on the reactor, as show in Fig 2, we have identified the state matrices A, B and C with the assistance of the sub-space method [26] as

$$A = \begin{bmatrix} -0.0019 & -0.00061 \\ 0.00098 & 0 \end{bmatrix}, B = \begin{bmatrix} 0.13 \\ 0 \end{bmatrix},$$

$C = [0, 0.18]$ and $n = 2$.

Note that the state x is unmeasurable, so we must use a state observer to estimate x, as shown in Fig. 3. More precisely,

$$\begin{aligned} \widehat{x}(t|t) &= \widehat{x}(t|t-1)+L'[y(t)-\widehat{y}(t|t-1)], \\ \widehat{x}(t+1|t) &= A\widehat{x}(t|t)+Bu(t), \\ \widehat{y}(t|t-1) &= C\widehat{x}(t|t-1), \end{aligned} \tag{2}$$

where $\widehat{x}$ is the estimate of x, $L' \in \mathbb{R}^{2\times 1}$ is the state observer gain, $*(t+i|t)$ means using the information available at time t to predict the value of $*$ at time $t+i$. By Kalman filter method [27], we obtain $L' = [0.0723, 0.0281]^\intercal$.

It follows from Eq. (2) that

$$\begin{aligned} \widehat{x}(t+1|t) &= (A-LC)\widehat{x}(t|t-1)+Bu(t)+Ly(t), \\ e(t+1) &= (A-LC)e(t) \end{aligned} \tag{3}$$

with $L := AL'$ and state estimate error $e(t) := x(t) - \widehat{x}(t|t-1)$. Thereby, the future dynamics can be iterated by recursively using Eq. (2) as below,

$$\begin{aligned} \widehat{x}(t+2|t) &= A^2\widehat{x}(t|t)+ABu(t|t)+Bu(t+1|t), \\ &\vdots \\ \widehat{x}(t+H_p|t) &= A^{H_p}\widehat{x}(t|t)+A^{H_p-1}Bu(t|t)+\cdots \\ &\quad +Bu(t+H_p-1|t), \end{aligned}$$

which can be rewritten by a compact form

$$Y(t) = F\widehat{x}(t)+GU(t) \tag{4}$$

with $u(t|t) = u(t)$, $\widehat{x}(t) = \widehat{x}(t|t)$ given in Eq. (2), $Y(t) = [y(t+1|t), y(t+2|t), \cdots, y(t+H_p|t))]^\intercal$, $U(t) = [u(t|t), u(t+$

This article has been accepted for publication in a future issue of this journal, but has not been fully edited. Content may change prior to final publication. Citation information: DOI 10.1109/TNANO.2015.2471298, IEEE Transactions on Nanotechnology

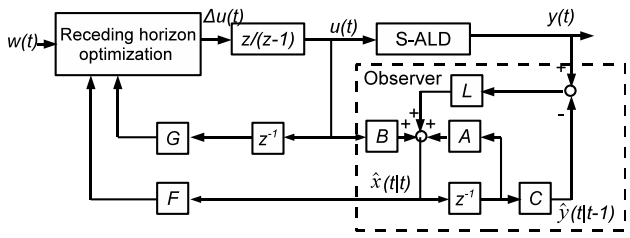

Fig. 3. Structure of the controller with a state observer.

$1|t), \cdots, u(t+H_u|t))]^\intercal$, $F = [CA, CA^2, \cdots, CA^{H_p}]^\intercal$,

$$G = \begin{bmatrix} CB & 0 & \cdots & 0 \\ CAB & CB & \cdots & 0 \\ \vdots & \vdots & \ddots & 0 \\ CA^{H_u-1}B & \cdots & \cdots & CB \\ \vdots & \vdots & \vdots & \vdots \\ CA^{H_p-1}B & \cdots & \cdots & CA^{H_p-H_u}B \end{bmatrix}_{H_p \times H_u}$$

and H_p, H_u are the prediction and control horizons, respectively.

B. GPC with Moving Substrate Disturbances

In the process of thin film deposition, the reactor is controlled to the target temperature by GPC under external disturbances. To this end, the control performance is quantified by a quadratic index as

$$\begin{aligned} J(t) &= \sum_{j=1}^{H_p}(y(t+j|t) - w(t+j))^2 \\ &\quad + \sum_{j=1}^{H_u} \lambda(\Delta u(t+j-1|t))^2 \end{aligned} \quad (5)$$

where $\lambda > 0$ is the weighting factor, incremental control law $\Delta u(t) := u(t) - u(t-1)$ and $w(t)$ is the reference signal. Note that the signal $w(t+j|t)$ denotes the future reference trajectory calculated by

$$w(t+j|t) = \alpha^j y(t) + (1-\alpha^j) r(t), j = 1, 2, \cdots, H_p, \quad (6)$$

where $r(t)$ is the set-point and $\alpha \in (0,1)$ is the softening factor to alleviate the aggressiveness of the control law [28]. Significantly, the first and second terms of the index $J(t)$ penalize the future temperature tracking error and the control cost, respectively. The incremental control law $\Delta u(t)$ can be solved by minimizing the index (5) for $\partial J(t)/\partial U(t) = 0$ as follows

$$\Delta u(t) = \eta(G^\intercal(t)G(t) + \lambda \mathbf{I}_{H_u})^{-1} G^\intercal(t)(\mathbf{w}(t) - F\widehat{x}(t)) \quad (7)$$

with $\eta := [1, 0, \cdots, 0]_{1\times H_u}$. The control signal $u(t) = u(t-1) + \Delta u(t)$ is transmitted to the PLC-DA module to heat the reactor.

In the control process, dynamics model mismatch inevitably exists between the state-space model (1) and the plant, especially under external disturbances. Recalling the fact that the moving speed determines the thin film deposition efficiency in the S-ALD system, the model mismatch is intensified by the variational rate from 0 to 15.0, then to 22.5, and finally to 27.5 mm/s. So online model identification and rectification become necessary, where the output matrix C in [1] is identified online by recursive least squares estimation (RLSE) based on the most recent input/output sequences as below,

$$\begin{aligned} \widehat{C}^\intercal(t) &= \widehat{C}^\intercal(t-1) + \Phi(t)[y(t) - \widehat{x}^\intercal(t|t)\widehat{C}^\intercal(t-1)], \\ \Phi(t) &= P(t-1)\widehat{x}(t|t)[\widehat{x}^\intercal(t|t)P(t-1)\widehat{x}(t|t) + \mu]^{-1}, \\ P(t) &= \tfrac{1}{\mu}\left[\mathbf{I} - \Phi(t)\widehat{x}^\intercal(t|t)\right] P(t-1). \end{aligned} \quad (8)$$

where $P(t) \in \mathbb{R}^{n\times n}$, $\Phi(t), C^\intercal(t) \in \mathbb{R}^n$, $\mu \in (0,1)$ is the forgetting factor, and the initial matrix $P(0)$ is set arbitrarily. Note that, by extensive experiments, it is verified that the online identification and adjustment of output vector C could absorb the model mismatch in the S-ALD processes. For more severe uncertainties in other cases, the sub-space method can be used to identify and update the state matrices A and B online.

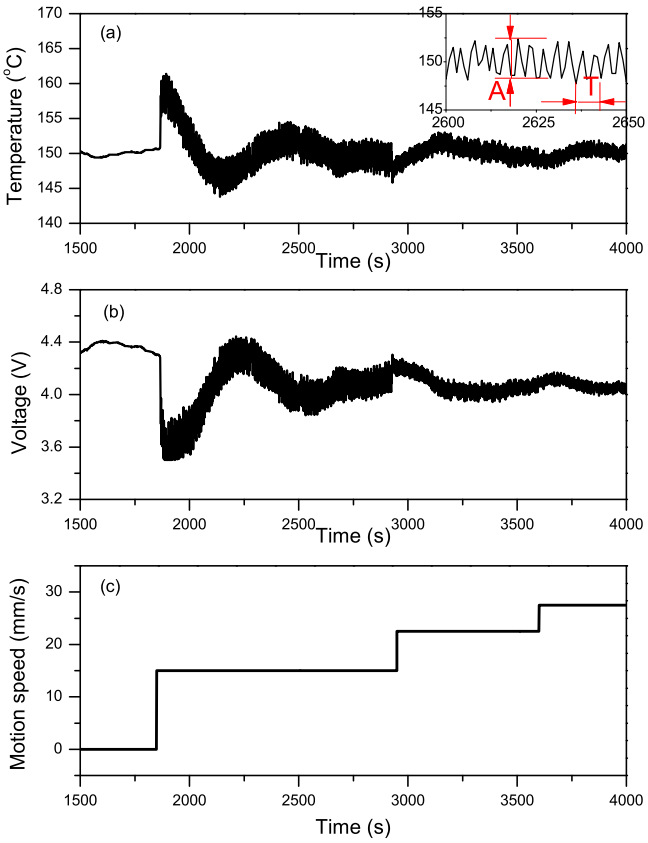

Fig. 4. Evolution of temperature $y(t)$ (a), control voltage $u(t)$ (b), and moving speed of the substrate (c) .

In the control experiments, all injectors are filled with 500 sccm nitrogen gas, respectively. It is observed in Fig. 4 that the substrate temperature y settles to the set-point value in the presence of external disturbances induced by the moving substrate with a variational speed. Specifically, the temperature y begins to oscillate once substrate moves, and the magnitude decreases with the increasing of moving speed. The temperature fluctuant magnitudes are 4.2, 2.8, and 2.3 $^\circ C$ corresponding to 15, 22.5 and 27.5 mm/s step speed disturbances. For example, when the speed is 15.0 mm/s, the fluctuation period is 6 s that is approximately equal to the substrate round trip time. These observations can be explained as follows. The

This article has been accepted for publication in a future issue of this journal, but has not been fully edited. Content may change prior to final publication. Citation information: DOI 10.1109/TNANO.2015.2471298, IEEE Transactions on Nanotechnology

mixture of carrier gas/precursor vapors and the inert gas are fed into the precursor and barrier areas, respectively, to form a gas flow layer within the long and narrow gap between the injector lower surface and the substrate. Moreover, the gas flow rate attains its peak value when it reaches the position under the injector inlet, and afterwards gradually decreases till reaching the outlet. Thus with the movement of the substrate, the gas flow cooling effect is variational.

Meanwhile, the motor switches the moving direction at both ends, which inevitably affects the reactor temperature as well. Interestingly, the observation that higher moving speed corresponds to lower temperature oscillation is due to the fact that the cooling time of gas flow is shorter under a certain gas flow distribution length. More precisely, a gas flow layer with high conductance is generated within the narrow gap between the injectors and the moving substrate in the S-ALD system. Usually, the gas flow rate under the injector zone is higher than those on the other positions. When the substrate passes through the injector zone faster, the heat loss due to the incoming gas flow is less. Therefore, the temperature fluctuation decreases with the increasing of moving speed. One may notice that in the inset of Fig. 4 (a), the period "T" labels a time length corresponding to twice of the function period. In the S-ALD system, two reaction areas of precursors are isolated by an inert gas barrier layer. The gas flow rate right under the injector is highest, where the temperature reaches the nadir due to the incoming gas cooling. In an entire ALD reaction, the substrate moves back and forth between two precursor injectors. Hence the period of temperature is twice as much as the function period.

C. GPC with/without Gas Flow

In order to investigate the causes of the chamber temperature oscillations, we conduct two experiments, with and without gas flow (500 sccm) under the same substrate speed at 22.5 mm/s, respectively. As shown in Fig. 5, the temperature oscillations of the former are larger than those of the latter. Note that, even without gas flow, the temperature still oscillates, due to the vibration of the substrate induced by the motor. But by comparison with the temperature oscillation caused by gas flow (4.2 $^{\circ}C$), the one caused by the substrate vibration (1.8 $^{\circ}C$) is less than half.

D. Comparison of GPC with PID at Large Flow Rate

Sometimes, a high flow rate over 500 sccm of the carrier and inert gas for diffusion barrier is required to prevent the ambient air into the reaction area. Yet, high flow rate will lead to larger temperature reduction when the substrate moves under the precursor injectors, and afterwards the temperature will try to recover as quickly as possible once leaving the injector inlets. The substrate temperature has larger oscillations under higher flow rate. Thereby, it becomes necessary to examine the temperature recovering efficiency and robustness of the proposed GPC system in the presence of high gas flow rate perturbations (e.g., 1000 sccm). To this end, the GPC performance is compared with routine PID control performance as follows.

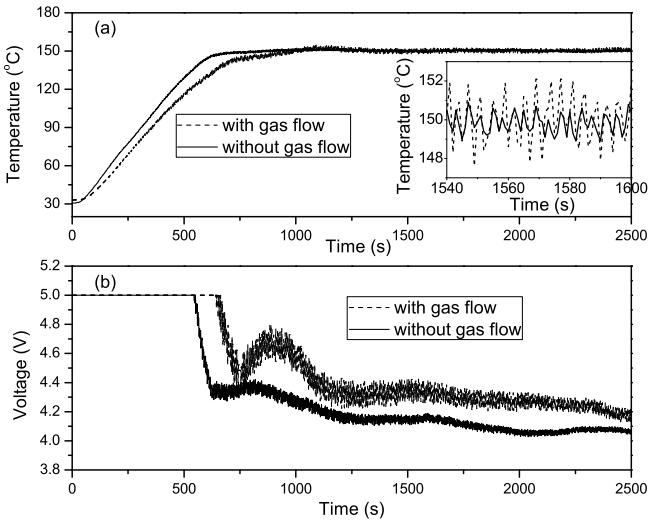

Fig. 5. Evolution of temperature $y(t)$ (a) and control voltage $u(t)$ (b) under a moving substate with or without gas flow.

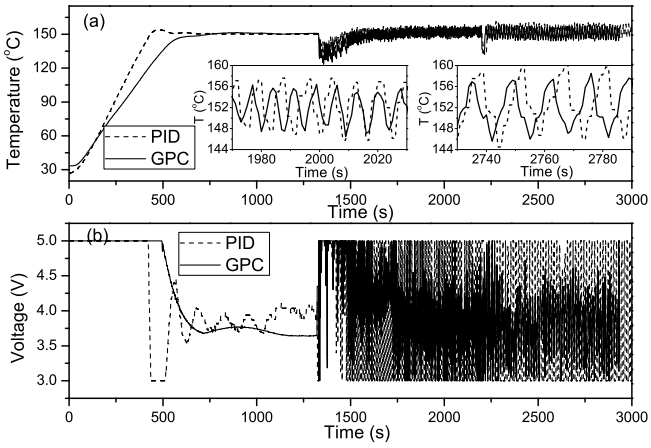

Fig. 6. Evolution of temperature $y(t)$ (a) and control voltage $u(t)$ (b) by GPC and PID. Here, in the 1350th second, both gas flow and substrate movement are introduced to the S-ALD platform.

We have conducted two groups of control experiments with different substrate motional types. The first one focuses on the film deposition efficiency, and hence the motor pauses for 1 s at the ends for direction switching. By contrast, the second group focuses on the thin film quality, so the substrate pauses for 2 s under the inert gas injector for excess gas purge, and is held for 2 s under precursor injectors for adequate chemical adsorption. The temperature $y(t)$ and control voltages $u(t)$ are shown in Fig. 6. Without the gas flow introduction and substrate movement, the setting times of PID and GPC are almost the same, which corresponds to the first deposition layer. But the overshoot (1.5 $^{\circ}C$) of GPC is much smaller than that of PID (4.0 $^{\circ}C$).

More significantly, when both gas flow and substrate movement are introduced at the 1350th second, both of the substrate temperatures of GPC and PID sharply decrease due to the gas cooling effect, and then recover to the set-point by the feedback controllers. It is observed in Fig. 6(a) that the temperature oscillations of GPC are remarkably smaller than the PID. To quantify the comparison, we calculate the standard

This article has been accepted for publication in a future issue of this journal, but has not been fully edited. Content may change prior to final publication. Citation information: DOI 10.1109/TNANO.2015.2471298, IEEE Transactions on Nanotechnology

deviation $\sigma := \sqrt{\frac{1}{N}\sum_{n_0}^{n_0+N-1}(y(k) - \frac{1}{N}\sum_{n_0}^{n_0+N-1} y(k))^2}$ of the steady-state temperatures of GPC and PID in 10 minutes with $n_0 = 1600$ and $N = 600$. It is observed that standard deviations of GPC and PID are $\sigma_g = 2.8\ ^\circ C$ and $\sigma_p = 3.5\ ^\circ C$ in the first experiment group, respectively, and $\sigma_g = 3.6\ ^\circ C$ and $\sigma_p = 4.2\ ^\circ C$ in the second experiment group, respectively. Therefore, GPC outperforms PID in dealing with gas flow and substrate movement disturbances. This advantage is due to the receding horizon optimization nature of GPC, which accommodates more system uncertainties and external disturbances than PID.

IV. Temperature Control Experiments to Deposit Nano-Laminate Films

For most experimental approaches depositing nano-laminate films, ALD reactions with different organometallic precursors often take place at the same target temperature to simplify the reactor structure and experimental technics under temporal batch-mode ALD systems. Thus only precursors with the overlap ALD temperature windows could be selected to form nano-laminates, which inevitably limits the choice of nano-laminat films. While in S-ALD systems, temperature controllers are capable of tracking variational temperature trajectories, and it is more desirable and feasible to fabricate multi-layer nano-laminates with different temperature windows.

A. Design of Temperature Switching Structure

The designed S-ALD can also be used to produce a nano-laminate film or a multi-element compound thin film. To this end, we could expand another unit B with injectors of precursors and inert gas by the pattern of $ABAB\cdots AB$ with flow chart given in Fig. 7. In the ALD A unit, the reaction forms thin film A with desired thickness. Afterwards, the substrate moves to position B in the ALD B unit. Once the substrate settles to the corresponding target temperature, the substrate moves back and forth between the precursor injectors to form the second layer B above the formed layer A within several cycles. Afterwards, the substrate can also be transmitted back from position B to position A upon the completion of ALD B deposition. By repeating such a process, a compound film is formed, where the two layers acts as an electronically functional device and a protective layer to reject the atmosphere, respectively. Alternatively, the nano-laminate film can be annealed to form multi-element compound, which has different properties like refractive index and dielectric constant, with different ratio of A with B [29]. Recalling that A and B units have different operational temperature ranges, their temperatures should be stabilized within the corresponding ranges to fulfill the film production technical requirement.

B. Switching Process Comparison between GPC and PID

We hereby investigate the temperature settling time (within $\pm$ 2 $^\circ C$ around the target temperature) of the switching process between different reactors during the nano-laminate film deposition. For simplicity, the heaters of ALD A and ALD B are set to 100 $^\circ C$ and 150 $^\circ C$, respectively. More precisely, compound A is formed with substrate temperature at 100 $^\circ C$, while compound B is added on the top of compound A with substrate temperature at 150 $^\circ C$. For conciseness, the temperatures of the substrate, holders A and B are denoted as y_S, y_A, and y_B, respectively.

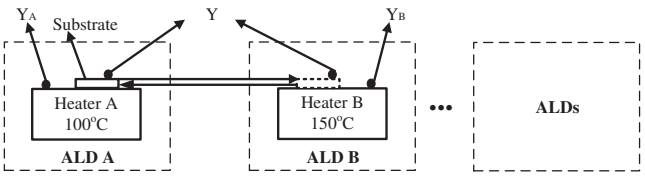

Fig. 7. Substrate switching process under different heaters with different ALD reactions.

In the ALD reactions, y_S is required to be stabilized at the set-point to activate the deposition reaction. When the substrate is in the unit A, the set-point of y_S is 100 $^\circ C$. Since the subsequent experiment will be conducted in unit B, y_B should be maintained at 150 $^\circ C$ in advance. Thus when the substrate moves into ALD B, y_S sharply increases to around 150 $^\circ C$, due to the good heat conductivity of the silicon substrate. However, owing to the unevenly distributed temperature field and the heat dissipation from the holder to the substrate, there exists a sharp temperature difference between y_B and y_S. Upon the switching, the set-point of the substrate therefore changes from 100 $^\circ C$ to 150 $^\circ C$ to calculate the control voltage for heater B. Meanwhile the temperature in ALD A should be kept at 100 $^\circ C$ to repeat the alternate nano-laminate structure, and hence y_A will be fed back to compute the control voltage for heater A. Returning to ALD A area after depositing compound B, the control voltage of heater B is calculated according to y_B and the set-point 150 $^\circ C$, while the control voltage of heater A is calculated based on y_S and the set-point 100 $^\circ C$.

As shown in Fig. 8, the substrate temperatures of both GPC and PID strategies experience oscillations around the set-point due to the balancing procedure of the heating and cooling effects, and then settle to the set-point. The settling times of GPC during the ascending and descending edges are 82 s and 79 s, respectively, which are much shorter than those of PID for 251 s and 226 s. In this way, the deposition efficiency is substantially improved by the present GPC scheme.

V. ALD Experiments

The deposition experiment of Al_2O_3 thin film is conducted in this section to verify the effectiveness of GPC temperature control system. The precursors are trimethyl-aluminum (TMA) and deionized water (18.2 MΩ). Ultrahigh purity nitrogen (99.999%) serves as the carrier gas and inert gas for diffusion barrier. A mixture with 15 sccm nitrogen and TMA vapor is diluted with 500 sccm nitrogen again, and then fed into the corresponding injector. First dilution nitrogen flow rate of the water vapor is 20 sccm. The injectors for diffusion barrier are filled with 500 sccm nitrogen, respectively. The substrate pauses 1 s under the precursor injectors, whose moving speed is set as 22.5 mm/s.

This article has been accepted for publication in a future issue of this journal, but has not been fully edited. Content may change prior to final publication. Citation information: DOI 10.1109/TNANO.2015.2471298, IEEE Transactions on Nanotechnology

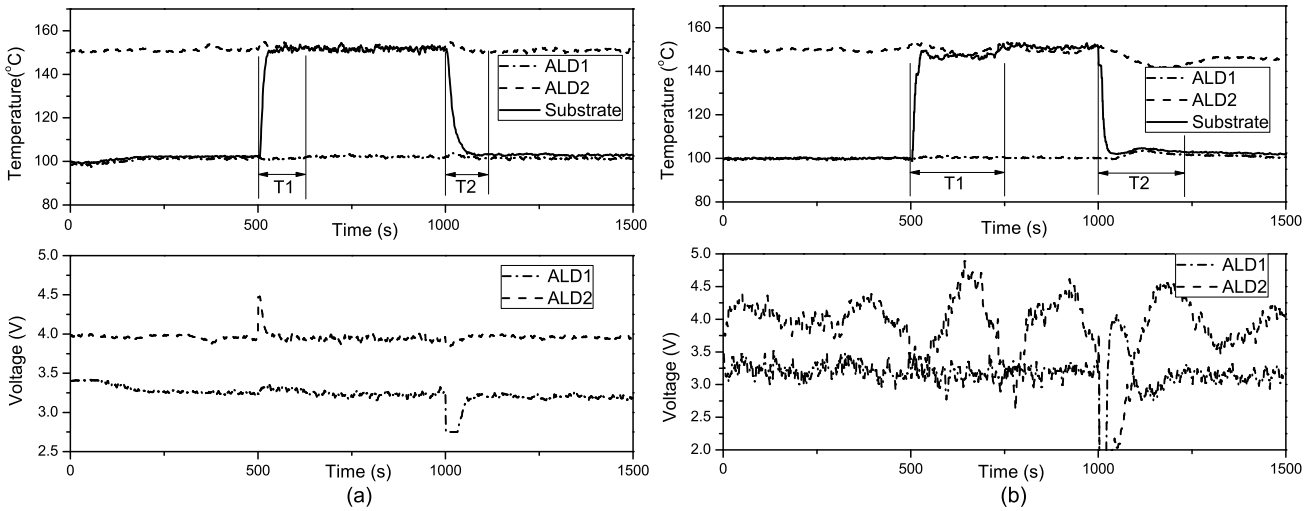

Fig. 8. Substrate temperature responses under two ALD reactors based on (a) GPC, (b) PID.

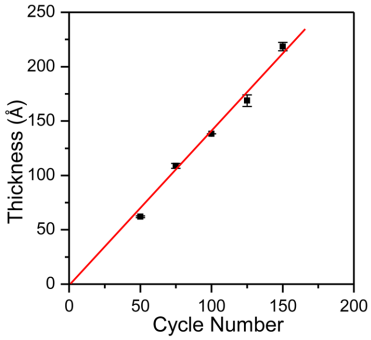

Fig. 9. Growth rate per cycle of thin film with different cycles.

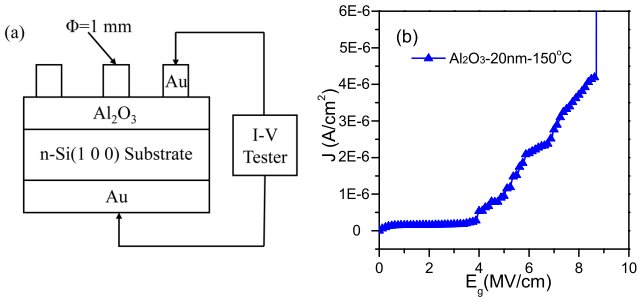

Fig. 10. (a) Structure of I–V measurement. (b) I–V characteristic curve of Al_2O_3 thin film.

ALD experiments are deposited with different cycle numbers (50, 75, 100, 125, and 150) to examine the growth rate. As shown in Fig 9, the film thickness is measured by a Spectroscopic Ellipsometry (SE, J.A. Woolman M2000). The growth rate per cycle of the Al_2O_3 thin film is 1.26 Å/cycle by linear fitting method, which is similar to the rate in literature of S-ALD system [30]. However, the average growth rate per cycle in S-ALD system is slightly larger than the one in conventional ALD reactor [16], since S-ALD system is in ambient air condition instead of vacuum, which is tougher to control the layer-by-layer growth and high quality films due to the fact that the trace amount of moistures and impurities in the atmosphere is hard to get rid of. The film producing rate could reach 1.1 Å/s with the stepper motor in our S-ALD reactor, which is about an order of magnitude higher than temporal ALD process. Note that the speed of the stepper motor is only 22.5 mm/s, while the linear motor could reach to a few hundred of mm/s. For TMA and water precursors, the surface absorption for saturation is within a few milliseconds, thus the moving speed determines film deposition rate. Furthermore, adding multiple serial precursor injector units, along with faster substrate moving speed, the deposition rate can be improved by 1–2 order of magnitudes [13].

Since Al_2O_3 ultra thin films are good insulators, current–voltage (I–V) characteristic test (Cascade Microtech SUMMIT 11000B-M) is performed to examine its dielectric constant and breakdown voltage. Gold (Au) is sputtered on the surface of Al_2O_3 to avoid film damage, and on the back of the n-Si(1 0 0) substrate, to act as the metallic contacts for I-V test as shown in Fig. 10(a). From Fig. 10(b), very low current density, of the order of μA/cm^2, is observed under the voltage imposing on the deposited film sample. The breakdown voltage density is 8.7 MV/cm under 20 nm oxide thickness, which is consistent with literature reports [8].

In order to explore how the temperature variation affects the quality of the deposited thin film, we conduct the ALD experiments with GPC and PID controllers, respectively. Atomic Force Microscopy (AFM, Agilent 5500) is performed in tapping mode to characterize the surface topography and roughness in an area of 1 μm $\times$ 1 μm. As shown in Fig. 11(a), the root-mean-square (RMS) of films for GPC and PID are 0.43 and 0.62 nm, respectively. Moreover in Fig. 11(b), the microstructure of the film under GPC is improved with smaller scanning voltage amplitude, which verifies the superiority of GPC, due to the adaptivity in the presence of disturbances.

ZnO is a poly-crystalline, conducting film with a rough surface topography, while Al_2O_3 is an excellent amorphous, insulating film with high conformality. Al_2O_3/ZnO nanolaminates may possess properties such as smooth surface and improved crystallinity [8, 31]. Here, we conduct experiments

This article has been accepted for publication in a future issue of this journal, but has not been fully edited. Content may change prior to final publication. Citation information: DOI 10.1109/TNANO.2015.2471298, IEEE Transactions on Nanotechnology

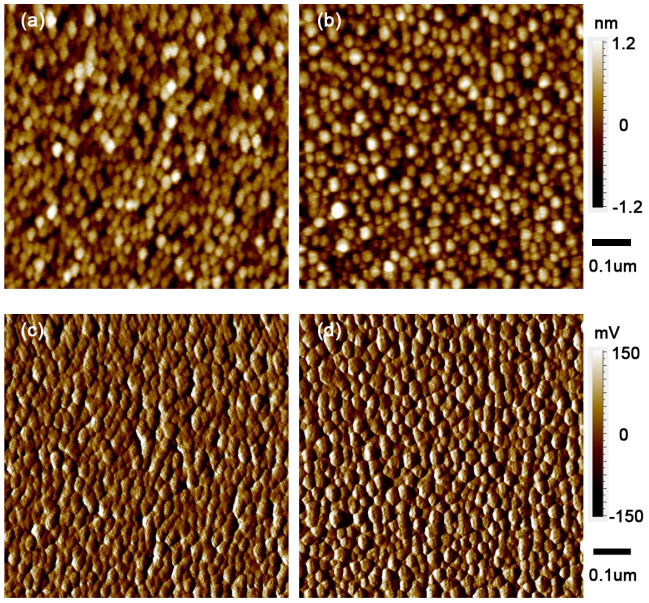

Fig. 11. AFM images of (a) GPC (b) PID, scanning amplitudes of (c) GPC (d) PID with Al_2O_3 thin film for 100 cycles.

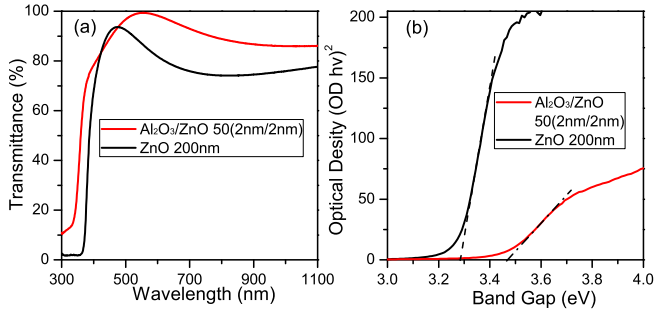

Fig. 12. (a) Transmittance spectra, (b) band gap of Al_2O_3/ZnO nano-laminate film and ZnO film.

of depositing nano-laminates to examine the developed S-ALD device with the present GPC controller. Therein, ALD A unit accounts for the deposition of Al_2O_3, while ALD B unit for ZnO deposited with precursors diethyl-zinc (DEZ) and deionized water (18.2 MΩ). A 2 nm Al_2O_3 layer is deposited above the glass substrate, above which a 2 nm ZnO layer is deposited. By repeating the procedure for 50 times, a nano-laminate is formed with thickness of 200 nm.

Optical characterization of Al_2O_3/ZnO nano-laminate film is obtained from UV–vis transmittance (Lambda 35 UV/VIS Spectrometer) with measurement spectral wavelength range of 300–1100 nm. The transmittance spectra of the Al_2O_3/ZnO nano-laminate with GPC-based closed-loop control system is shown in Fig. 12(a), and compared with the 200 nm ZnO film. It is observed that the transmittance of Al_2O_3/ZnO is 8–15% higher than pure ZnO in the common transparent zone 550–1100 nm. Meanwhile, as shown in Fig. 12(b) deriving from Fig. 12(a), the optical band gap 3.47 eV of Al_2O_3/ZnO nano-laminate with GPC is larger than the gap 3.36 eV of ZnO film. This presents the optical transmittance wavelength range is from $1240/3.47$ = 357 nm to 1100 nm for nano-laminate, which is wider than the range [378, 1100] nm for ZnO film. Recalling Section IV, the settling and switching times with GPC controller are shorter than with PID controller in depositing nano-laminate films under different temperature windows, which largely improves the processing efficiency. Thus the feasibility and superiority of the developed S-ALD reactor with GPC controller is verified.

VI. Conclusion

This paper established an S-ALD platform and developed a closed-loop reactor temperature control system based on GPC strategy. The merits of the developed controller lied in short settling time and robustness to both system uncertainties and external disturbances induced by the substrate movement and the gas flows. In comparison with the PID strategy routinely used in ALD processes, extensive experimental results verified the attenuated temperature oscillations and reduced settling time. The good I-V characteristics and optical transmittance verified the feasibility of the developed GPC system. Thereby, compared to PID system, both the microstructure of the deposited ALD thin film and the production efficiency were improved by the proposed GPC system.

Acknowledgment

The authors would like to thank Y.-L. Gao, Z. Deng, and C.-L. Duan for the assistance of establishing the S-ALD reactor. The authors would also like to acknowledge equipment supports from AMETEK lab, laboratory of School of Mechanical Science and Engineering, and the technology support by the Analytic Testing Center of HUST.

References

[1] S. M. George, "Atomic layer deposition: an overview," *Chemical Reviews*, vol. 110, pp. 111–131, 2010.

[2] A. W. Ott, S. M. George, and J. W. Klaus, "Surface chemistry for atomic layer growth," *Joural of Physical Chemistry*, vol. 100, pp. 13121–13131, 1996.

[3] R. B. Clark-Phelps, O. Sneh, A. R. Londergan, J. Winkler, and T. E. Seidel, "Thin film atomic layer deposition equipment for semiconductor processing," *Thin Solid Films*, vol. 402, pp. 248–261, 2002.

[4] X. Du and S. M. George, "Thickness dependence of sensor response for CO gas sensing by tin oxide films grown using atomic layer deposition," *Sensors and Actuators B: Chemical*, vol. 135, pp. 152–160, 2008.

[5] A. C. Dillon, A. W. Ott, J. D. Way, and S. M. George, "Surface chemistry of Al_2O_3 deposition using $Al(CH_3)_3$ and H_2O in a binary reaction sequence," *Surface Science*, vol. 322, pp. 230–242, 1995.

[6] R. Chen, H. Kim, P. C. McIntyre, and S. F. Bent, "Self-assembled monolayer resist for atomic layer deposition of HfO_2 and ZrO_2 high-k gate dielectrics," *Applied Physics Letters*, vol. 84, no. 20, pp. 4017–4022, 2004.

[7] R. Chen and S. F. Bent, "Chemistry for positive pattern transfer using area-selective atomic layer deposition," *Advanced Materials*, vol. 18, pp. 1086–1090, 2006.

[8] A. A. Chaaya, R. Viter, I. Baleviciute, M. Bechelany, A. Ramanavicius, Z. Gertnere, D. Erts, V. Smyntyna,

and P. Miele, "Tuning optical properties of Al_2O_3/ZnO nanolaminates synthesized by atomic layer deposition," *The Journal of Physical Chemistry C*, vol. 118, no. 1, pp. 3811–3819, 2014.

[9] P. Poodt, D. C. Cameron, E. Dickey, S. M. George, V. Kuznetsov, G. N. Parsons, F. Roozeboom, G. Sundaram, and A. Vermeer, "Spatial atomic layer deposition: A route towards further industrialization of atomic layer deposition," *Journal of Vacuum Science and Technology A*, vol. 30, no. 1, pp. 010802–1–11, 2012.

[10] D. H. Levy, D. Freeman, S. F. Nelson, P. J. Cowdery-Corvan, and L. M. Irving, "Stable ZnO thin film transistors by fast open air atomic layer deposition," *Applied Physics Letters*, vol. 92, no. 19, pp. 192101–1–3, 2008.

[11] A. Illiberi, F. Roozeboom, and P. Poodt, "Spatial atomic layer deposition of zinc oxide thin films," *ACS Applied Materials and Interfaces*, vol. 4, no. 1, pp. 268–272, 2012.

[12] V. I. Kuznetsov, E. H. A. Granneman, P. Vermont, and K. Vanormelingen, "High throughput ald of Al_2O_3 layers for surface passivation of silicon solar cells," *ECS Transactions*, vol. 33, no. 2, pp. 441–446, 2010.

[13] P. Poodt, A. Lankhorst, F. Roozeboom, K. Spee, D. Maas, and A. Vermeer, "High-speed spatial atomic-layer deposition of aluminum oxide layers for solar cell passivation," *Advanced Materials*, vol. 22, no. 36, pp. 3564–3567, 2010.

[14] A. Illiberi, R. Scherpenborg, P. Poodt, and F. Roozeboom, "Spatial atomic layer deposition of transparent conductive oxides," *ECS Transactions*, vol. 58, no. 10, pp. 105–110, 2013.

[15] D. H. Levy, S. F. Nelson, and D. Freeman, "Oxide electronics by spatial atomic layer deposition," *Journal of Display Technology*, vol. 5, no. 12, pp. 484–494, 2009.

[16] W.-J. He, H.-T. Zhang, Z. Chen, B. Chu, K. Cao, B. Shan, and R. Chen, "Generalized predictive control of temperature on an atomic layer deposition reactor," *IEEE Transaction on Control Systems Technology, DOI 10.1109/TCST.2015.2404898*.

[17] N. N. Qi, Y. C. Fang, X. Ren, and Y. N. Wu, "Varying-gain modeling and advanced DMPC control of an AFM system," *IEEE Transaction on nanotechnology*, vol. 14, no. 1, pp. 82–92, 2015.

[18] M. S. Rana, H. R. Pota, and I. R. Petersen, "High-speed AFM image scanning using observer-based MPC-notch control," *IEEE Transaction on nanotechnology*, vol. 12, no. 2, pp. 246–254, 2013.

[19] S. J. Qin and T. A. Badgwell, "A survey of industrial model predictive control technology," *Control Engineering Practice*, vol. 11, pp. 733–764, 2003.

[20] H.-T. Zhang, Z. H. Chen, Y.-J. Wang, T. Qin, and M. Li, "Adaptive predictive control algorithm based on laguerre functional model," *International Journal of Adaptive Control Signal Process*, vol. 20, no. 2, pp. 53–76, 2006.

[21] H.-T. Zhang, G. Chen, and M. Z. Q. Chen, "A novel dual-mode predictive control strategy for constrained wiener systems," *International Journal of Robust and Nonlinear Control*, vol. 20, pp. 975–986, 2009.

[22] D. Q. Mayne, J. B. Rawlings, C. V. Rao, and P. O. M. Scokaert, "Constrained model predictive control: stability and optimality," *Automatica*, vol. 36, pp. 789–814, 2000.

[23] D. W. Clarke, C. Mohtadi, and P. S. Tuffs, "Generalized predictive control. part 1: The basic algorithm," *Automatica*, vol. 23, pp. 138–148, 1987.

[24] M. Alpbaz, H. Hapoglu, and G. Ozkan, "Experimental application of generalized predictive control of the temperature in a polystrene polymerization reactor," *Chemical Engineering Communications*, vol. 191, no. 9, pp. 1173–1184, 2004.

[25] E. F. Camacho and C. Bordons, *Model Predictive Control*. Springer London Ltd, 2nd ed., 2013.

[26] P. V. Overschee and B. L. R. D. Moor, "N4SID: Subspace algorithms for the identification of combined deterministic-stochastic systems," *Automatica*, vol. 30, no. 1, pp. 75–93, 1994.

[27] R. E. Kalman, "A new approach to linear filtering and prediction problems," *Journal of Basic Engineering*, vol. 82, no. 1, pp. 35–45, 1960.

[28] J. M. Maciejowski, *Predictive control: with constraints*. Prentice Hall, 2002.

[29] J. W. Elam and S. M. George, "Growth of ZnO/Al_2O_3 alloy films using atomic layer deposition techniques," *Chem. Mater.*, vol. 15, no. 4, pp. 1020–1028, 2003.

[30] M. B. M. Mousa, C. J. Oldham, and G. N. Parsons, "Atmospheric pressure atomic layer deposition of Al_2O_3 using trimethyl aluminum and ozone," *Langmuir*, vol. 30, no. 13, pp. 3741–3748, 2014.

[31] J. W. Elam, Z. A. Sechrist, and S. M. George, "ZnO/Al_2O_3 nanolaminates fabricated by atomic layer deposition: growth and surface roughness measurements," *Thin Solid Films*, vol. 414, no. 1, pp. 43–55, 2002.